

Tri-axis Convective Accelerometer with Closed-Loop Heat Source

Van Thanh Dau^{1*}, Thien Xuan Dinh,² Lam Bao Dang³, Canh-Dung Tran⁴, Tung Thanh Bui,⁵ and Phan Thanh Hoa^{6*}

¹Research Group (Environmental Health), Sumitomo Chemical. Ltd, Hyogo, 665-8555, Japan

²Graduate School of Science and Engineering, Ritsumeikan University, Kyoto, 525-8577, Japan

³School of Mechanical Engineering, Hanoi University of Science and Technology, Viet Nam

⁴School of Mechanical and Electrical Engineering, University of Southern Queensland, Queensland QLD 4350, Australia

⁵University of Engineering and Technology, Vietnam National University, Hanoi, Vietnam

⁶HaUI Institute of Technology, Hanoi University of Industry, Hanoi, Vietnam

*Corresponding authors: dauv@sc.sumitomo-chem.co.jp ; phanthanhhoa@haui.edu.vn

Abstract

In this paper, we report the details and findings of a study on tri-axis convective accelerometer, which is designed with the closed-loop type heat source and thermal sensing hotwire elements. The closed-loop heat source enhances the convective flow to the central part where a hotwire is placed to measure the vertical component of acceleration. The simulation was conducted using numerical analysis, and the device was prototyped by additive manufacturing. The device, functioning as a tilt sensor and an accelerometer, was tested up to acceleration of 20g. The experiments were successfully conducted and the experimental results agreed reasonably with those obtained by numerical analysis. The results demonstrated that the closed-loop heat source could reduce the cross effect between the acceleration components. The scale factor and cross-sensitivity had the values of 0.26 $\mu\text{V/g}$ and 1.2%, respectively. The cross-sensitivity and the effects of heating power were also investigated in this study.

Keywords: convective accelerometer, tri-axis, closed-loop heater, hotwire, OpenFOAM.

I. INTRODUCTION

Recently, micromachined accelerometers have undergone rapid development, and are widely used in various applications. Solid-state accelerometers have high performance, but also possess some setbacks. They are more fragile, fabricated by complicated process, and need complex packaging in order to remove the squeeze film effect between the proof mass and the accelerometer structure [1]. In Refs. [2], [3], the authors presented the first accelerometers without the proof mass, working under the principles of thermal convection heat transfer. Micro thermal convective accelerometers utilizing thermal bubble have been studied over the last two decades [4]. The operation of this type of sensor is based on the movement of a hot tiny air bubble generated from a heater. From then on, research has been carried out with focus on improving the sensor performance by optimizing the heat transfer [5–25], signal conditioning [26–28], behavior modelling [29–32], or fabrication process [33–35].

Most of the developed thermal accelerometers can measure only two components of the in-plane acceleration. Measuring the out-of-plane acceleration is more challenging because the principle of this kind of sensors is based on natural convective flow, which always aligns with the vertical gravity. Thus, the vertical acceleration requires an out-of-plane structure and has small sensitivity.

Leung et al. reported one of the first tri-axis accelerometers. The device is made by polyimide and assisted by wire bonding process for out-of-plane structure [36]. In Ref. [37], the accelerometer is made by micromachining process utilizing polysilicon as the sacrificed layer and polyimide as the structural layer. To launch the device, the

structures firstly need to be locked between each other and anchored to the substrate. This device allows obtaining the Z sensitivity of $25 \mu\text{V/g}$.

In the works published by Rocha and Silva [38–41], a polymeric three-axis device was fabricated by conventional micromachining and injection molding. The heating and the temperature sensing structures, made of aluminum, were patterned on a flexible polymeric membrane. The membrane was then folded so that parts of the membrane consisting of z-sensors were placed above and under the central part, which consisted of the heater and the in-plane x-y sensors. The device with performance of approximately $2.2 \mu\text{V/g}$ was packaged using polystyrene parts made by injection molding, and was hermetically sealed.

The Z-axis acceleration detected by in-plane structure was reported by Mailly et al. in [42,43] using integrated CMOS (complementary metal–oxide–semiconductor). This device measures out-of-plane acceleration by using common mode of the in-plane structure. MEMSIC Inc. has also claimed a three-axis device. However, the principle is not disclosed, although it is said that the device uses the common mode of the electric bridge [4,44]. Another principle for the triple-axis accelerometer has been proposed in [45] but without further discussion about efficiency. In Refs. [46,47], the design of three-axis thermal accelerometer using segmented circular heater was mentioned. Using numerical simulation, Ogami et al. reported that the sensor could reliably determine a vast range of vertical acceleration, specifically, $\pm 10,000 \text{ g}$ [47]. However, the experimental details were omitted.

As already mentioned above, it is difficult to detect the acceleration in the z-direction accurately. For measuring this acceleration, the temperature detecting components need to be arranged above and below the heater. When acceleration occurs, the detected temperatures change, but only by small amount. It has been found that the Z-axis detection accelerometer has a close relation with the natural convection of the flow inside a cavity heated from below [48–53]. In recent years, many researchers have found that boundary conditions [48,49] and heater geometry [50,51] have substantial impact on the pattern of these convective flows. Because of the temperature distribution, the local heating of the quiescent air over the heater surface produces density gradient directed toward the decrease in the medium temperature, and convective flow occurs in the form of thermal plume when the buoyancy exceeds the viscous friction [53]. For a single local heater under heating conditions, the hot air rises upwards along the vertical axis going through the heater. Therefore, the convective flow has high stability in the plane of the heater, but is less stable in the vertical direction [54]. These characteristics of flow from the plate-type heater usually employed in convective accelerometer reduce the sensitivity of the vertical acceleration sensing. Another setback is the interference between the measured acceleration components. Because of arrangement of the temperature detectors, when the acceleration in one direction causes a change in the corresponding temperature, it also affects the temperature elements of the remaining directions and distinctly lowers the measurement accuracy.

In this paper, we demonstrate a novel approach to develop a tri-axis convective accelerometer with reduced cross effect between the vertical and horizontal acceleration. This design, inspired by the numerical simulation in [55], involves development of accelerometer utilizing the ring-type heat source. The designed device consists of a closed-loop heater with hotwires placed both inside and outside of the heater. The closed-loop heater enhances the convective flow to the central part, where the temperature detector is positioned to measure the vertical component of acceleration. Outside the loop, other hotwires detect the horizontal components. The characteristics of the sensor are experimentally validated by tilting the device and by applying linear acceleration. The principles of the device, numerical simulation, and the effect of several governing parameters are also explored to investigate the reliability of the device.

II. WORKING PRINCIPLE

In general, the principle of acceleration sensing can be summarized as follow. The sensing chip, formed by one heater placed at the center and surrounded by hotwires (temperature detector), is packed in an airtight chamber. At the initial state, the heater creates a symmetrical temperature profile inside the chamber. When the device is subjected to acceleration, the locally heated air moves in the direction of this applied acceleration, causing

temperature distortions ΔT , which are then sensed by the hotwires. For horizontal measurement a_x or a_y , the output of sensor is given by ΔT_x or ΔT_y at the X or Y hotwires, respectively (Fig. 1a). For vertical measurement, the output is determined by the output of ΔT_z at the Z hotwire.

In most of the conventional accelerometers reported in the first section, the heater is suspended at the center and the hotwires are located around the heater. Consequently, the change in temperature caused by the variation of the vertical acceleration is low in comparison with that caused by the variation of the horizontal acceleration, and the cross-sensitivities between these measurements are high. In our design shown in Fig. 1, the heater forms a full loop and the hotwires are located both inside and outside of the heater. The plane of the hotwires has a small elevation from the heater plane for vertical and horizontal measurements.

In the closed-loop heater, the primary flow concentrates strongly within the central portion even if heat is not supplied there [56,57]. The high temperature air is concentrated in the central part, except in a very thin layer above the heat source. As this concentrated hot air has high buoyancy, the temperature varies with the vertical acceleration a_z . This increases the sensitivity of the vertical measurement significantly and reduces the cross-effect of horizontal acceleration, which is one of the limits of the conventional design.

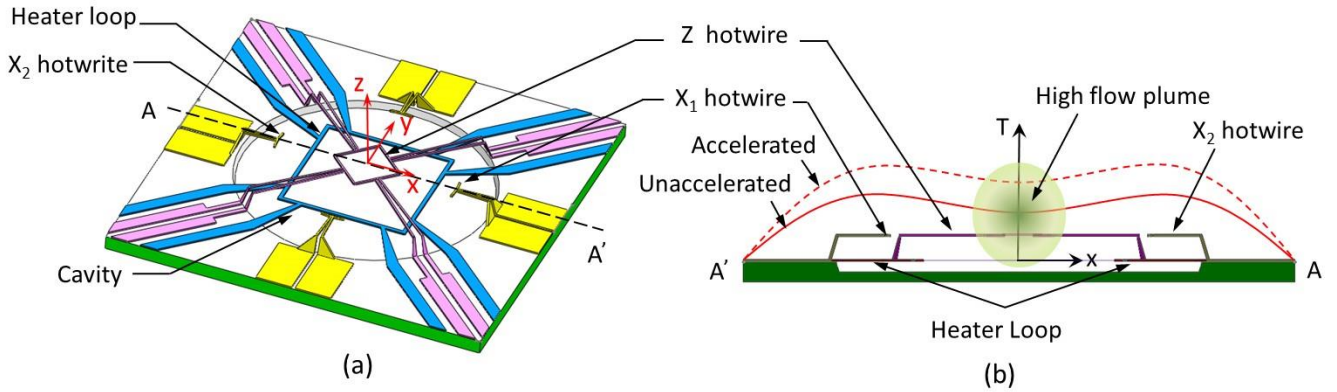


Figure 1. (a) Configuration of the sensor with the radius of the cavity of 0.75 mm. (b) Position of the hotwires in the cross section along the A–A' axis and principle to measure the vertical acceleration. The hotwires are on the same plane, and the heater is underneath. The Z hotwire is above the central portion of the heater to utilize convectively heated air from the ring-type heater.

III. SIMULATION AND DESIGN

The thermofluidic phenomena in the sensor are described by the temperature dependence of the fluid density. This process is governed by the laws of conservation of mass, momentum, and energy for compressible fluids and is expressed as follows:

$$\frac{\partial \rho}{\partial t} + \nabla \cdot (\rho \vec{u}) = 0 \quad (1)$$

$$\frac{\partial \rho \vec{u}}{\partial t} + \nabla \cdot (\rho \vec{u} \vec{u}) = -\nabla p + \nabla \cdot (\mu \nabla \vec{u}) + \rho \vec{a} \quad (2)$$

$$\frac{\partial \rho c_p T}{\partial t} + \nabla \cdot (\rho c_p T \vec{u}) = \nabla \cdot (\lambda \nabla T) \quad (3)$$

where \vec{u} and p are velocity and pressure of the fluid flow, respectively. Similarly, ρ , c_p , μ and λ are density, specific heat, viscosity, and thermal conductivity of the fluid, respectively. The term \vec{a} is the acceleration vector, while $\rho \vec{a}$ represents the momentum source because of the change in fluid density. As air is the medium in this study, the ideal gas law for compressible flows is valid. This can be stated as

$$p = \rho RT / M_w \quad (4)$$

where R is the universal gas constant and M_w is the molecular weight of the gas.

The sensor is decomposed into a hexagonal mesh clustered near the heater and walls to capture the steep change of temperature. The flow parameters on this mesh are then obtained by the computational fluid dynamics package OpenFOAM, which uses the finite volume method to discretize the governing equations. The simulation model is presented in Fig. 2.

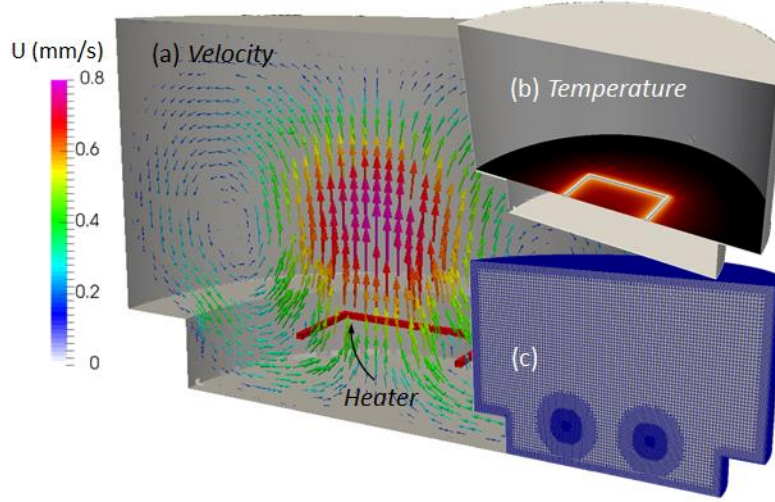


Figure 2. (a, b) Simulation results and (c) meshing of the model. Simulation shows that (a) flow velocity concentrates within the region above the center of ring-type heater while (b) the temperature is highest at the thin layer around the heat source.

From the simulation, it can be seen that the high temperature air is formed in the central portion above the heater except a thin layer around the heat source and the peak of temperature is distributed toward the center of the rim. For the velocity, the main part of the convection is strongly concentrated in the central part of the heater where no heat is supplied at the bottom. By placing a sensing element in this region, the specific character of the closed-loop type heater allows efficient measurement of the vertical acceleration and reduces the cross-effect of the horizontal acceleration. All of these phenomena will be discussed in the following paragraphs.

Considering the earth's gravity g , we discuss the sensor performance by comparing the initial state $a(0, 0, 1 \text{ g})$ and the accelerated state $a(a_x, a_y, a_z - 1 \text{ g})$. Because of the equivalency between the x and y components, only the measurements of x and z components of acceleration are taken into consideration. The sensitivity of the sensor can be determined from ΔT_x and ΔT_z , which are the temperature changes at the X hotwire and Z hotwire when the accelerations are applied on the X and Z axes, respectively. The cross-effect between the vertical and horizontal measurements is determined by ΔT_{xz} on the X hotwire under the effects of a_z and by ΔT_{zx} on Z hotwire under the effects of a_x . In the simulation, the sensitivity and cross-effect are examined by simultaneously applying a_x and a_z .

Figure 3 shows that the variation in temperature differences on the X hotwire (ΔT_x) with a_x , ranging from 0 g – 20 g, for the cases of $a_z = 1 \text{ g}$ and $a_z = 21 \text{ g}$. It is observed that ΔT_x varies linearly with a_x with the sensitivity $\Delta T_x / a_x \sim 0.29 \text{ }^\circ\text{C/g}$. The effect of a_z on ΔT_x , error $\Delta T_{xz}(\%) = (\Delta T_{x,az=21g} - \Delta T_{x,az=1g}) / \Delta T_{x,az=21g}$, is within 5% (in comparison with ΔT_x at $a_z = 1 \text{ g}$).

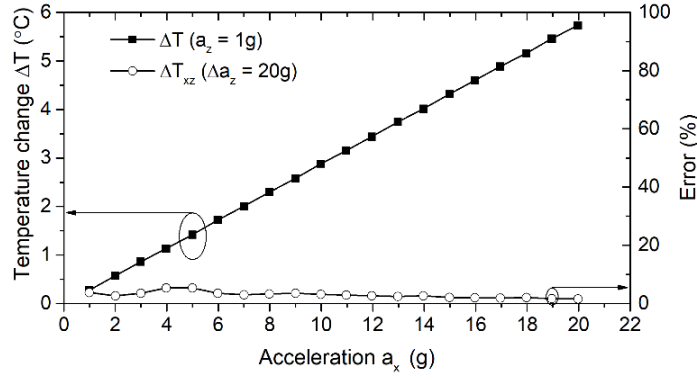


Figure 3. Variation of the temperature difference between the hotwires X_1 and X_2 for a_x ranging from 1 to 20 g. The error represents the percentage of temperature change ΔT_{zx} between $a_z = 21$ g and $a_z = 1$ g.

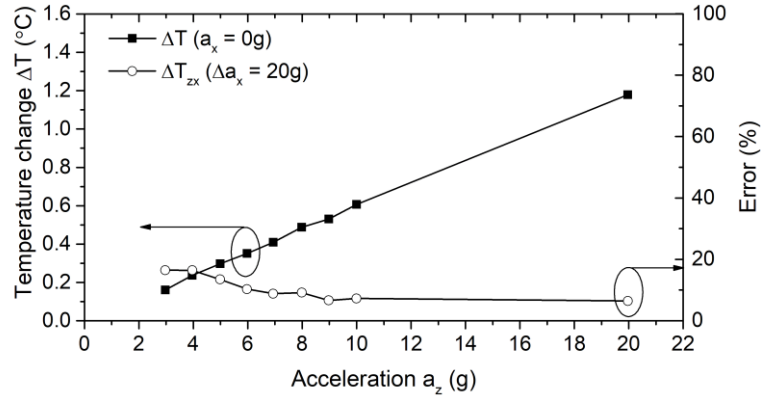


Figure 4. Variation of the temperature difference between the accelerated state and the normal state at the Z detector, with a_z ranging from 1 to 20 g. The error represents the percentage of temperature change ΔT_{zx} between $a_x = 20$ g and $a_x = 0$ g.

Similarly, for cases of $a_x = 0$ g and $a_x = 20$ g, Fig. 4 shows the change of temperature on Z hotwire (ΔT_z) with a_z . Again, ΔT_z increases linearly with a_z up to $a_z = 20$ g with the sensitivity $\Delta T_z/a_z \sim 0.059$ °C/g.

With α as the temperature coefficient of resistance of the hotwire material, the conversion between the hotwire temperature and its resistance can be expressed as:

$$R = R_{ref}(1 + \alpha \Delta T) \quad (5)$$

where $\Delta T = T - T_{ref}$, R , and R_{ref} are the resistances of the hotwire at temperature T and T_{ref} , respectively. In the experiment, the resistance is measured by supplying a constant direct current (d.c) and monitoring its voltage.

IV. PROTOTYPE AND EXPERIMENTAL SETUP

The sensor designed for the experiment consisted of top and bottom parts (Fig. 5a), which were connected as the male-female components of an assembly, to prevent the leakage of the air, which was used as the working medium in this device. The top view showing the layout of the hotwires and the heater is presented in Fig. 5b. The dimensions 10 mm × 10 mm × 8 mm (width × length × thickness) of the fabricated device are chosen based on several designs available for the dual axis convective accelerometer and the consideration of our available facilities [12]. The hotwire and heater were made of tungsten wire with diameter 10 μm. To place these elements at the desired positions, hollow capillary gold (Au) pipes 200 μm × 25 μm (outer diameter × thickness) were used as the

lead pins. The capillaries were assembled with the packing and fixed with epoxy glue; the tungsten wires were then inserted through those capillaries and connected with each other. Together they created floating structures. This method allowed the construction of the sensor with high precision and cost-effectiveness.

Figure 6a shows the prototype made of polypropylene. The heaters were supported by four Au pipes and were integrated with the bottom part. The hotwires were connected to the top part, where each X and Y hotwire was supported by two Au pipes at its end. The Z sensor and the heater were supported by four Au capillaries to form a loop-like resistor. The positioning of the capillaries was assisted by assembly jig (not shown). After the hotwires were connected and the electrical connections were confirmed, the top and bottom part were assembled and sealed by epoxy at the standard room condition (22–25 °C, 60% RH).

The temperature coefficient of resistance was measured as $\alpha \approx 4500 \text{ ppm}/^\circ\text{C}$ using the temperature controlled chamber (Espec SH-222). **Without conditioning circuit, the measurement of the hotwire/heater was conducted by four-point probe measuring technique. A constant electric current was applied by the TEXIO DC power source (PW18-1.8AQ) and the output voltage was continuously recorded by a computer via NI (National Instrument Ltd.,) signal express data logging interface connected to the NI-9234 data acquisition device with the sampling rate of 25.6 kHz.** At the initial state, the measured resistance values of the hotwires X, Y, Z, and heater were 1.7, 1.9, 1.2, and 1.3 Ω , respectively.

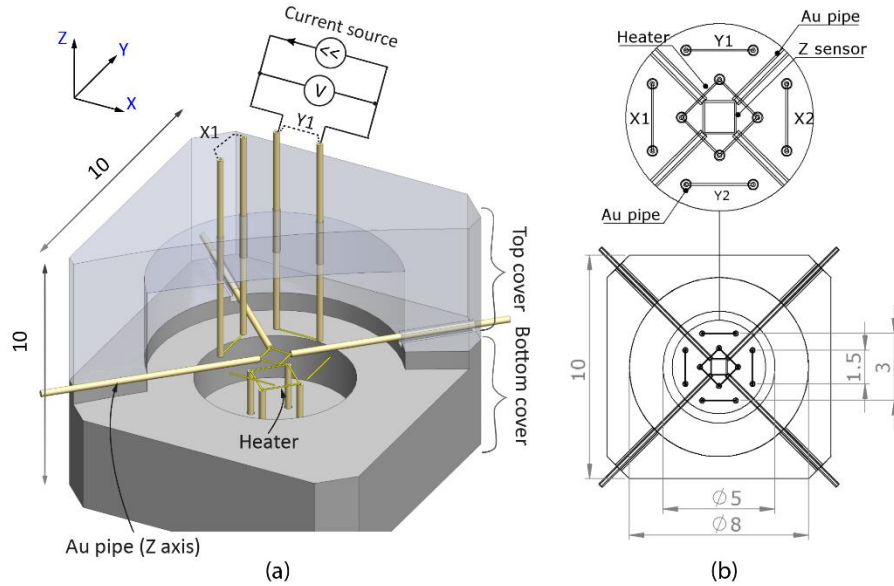


Figure 5. (a) Schematic view of the designed prototype with the cut-view showing the lead pin (made by Au capillary) and hotwires. (b) Dimensions of the central regions.

The sensing performance of the device was checked by the tilting test and linear acceleration test. For the tilting test, the device was attached to a circular disc placed vertically and tilted around the X and Y axes, while the voltages on the hotwires X, Y and Z were read out (see Fig. 6c).

The linear acceleration sensing was tested by placing the device at the edge of a self-developed turntable (see Fig. 6b), whose angular velocity was controlled by a direct current motor with integrated encoder (Tsukasa Electric Ltd.). When the turntable rotated, the centrifugal acceleration acted to the device was $a = (2\pi n)^2 r_t$, with n and $r_t = 4.5 \text{ cm}$ were the angular speed and radius of the turntable, respectively. The on-chip circuit was connected via the slip-ring to the off-chip circuit to transfer the signals while the turntable rotated. The table revolution had a maximum value of 700 rpm during the experiment, and its rotation was recorded by the PIC18F4520 microcontroller via encoder motor. **The output voltage was extracted one minute after the turntable reached the rotation speed to ensure that the centrifugal acceleration and the flow inside device were stable.**

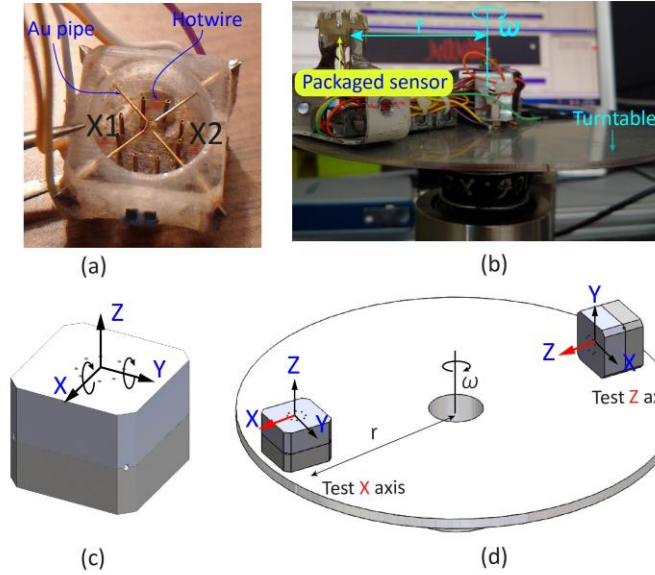


Figure 6. (a) Close-up view of the prototype showing hotwires and Au pipes, (b) package device with holder placed on the turntable, (c) tilting test: experiment for determining tilting along the X and Y axes, and (d) linear acceleration test: experiment for determining centrifugal acceleration along the X and Z axes.

The start-up time of the device was acquired from the transient time of the output voltage on the hotwire X (plotted in Fig. 7). It was found that the start-up time was around 100 ms for the X axis, which was located 1.0 mm from the heater, with the applied current of heater $I_{heater} = 110\text{mA}$ ($V_{heater} = 0.177\text{ V}$). This start-up time, including the time delay in the electric circuit, also represented the time scale for heat transfer from the heater to the hotwire until the temperature in the sensor chamber became stable.

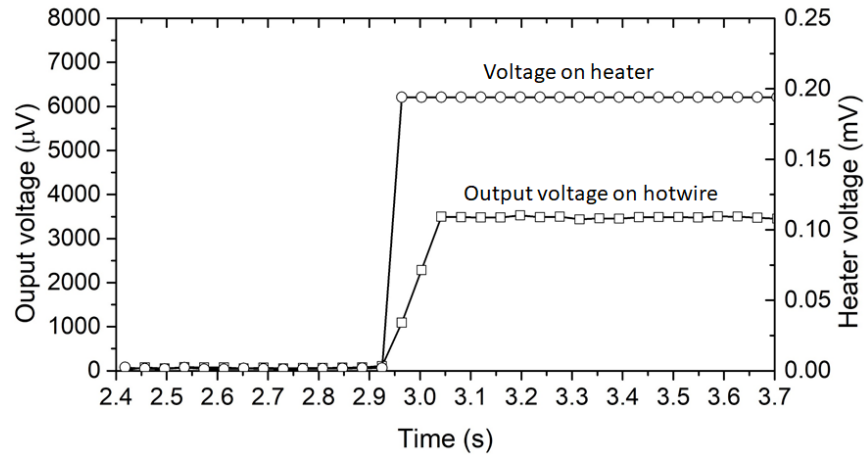


Figure 7. Experimental result for the transient measurements of voltages on the heater and the hotwire X.

V. EXPERIMENTAL RESULT

1. Tilting sensitivity of X and Y axes

For the tilting test, the outputs of hotwires were monitored while the sensor was being rotated to ensure that the corresponding hotwire moved from underneath the heater to the top of the heater. In Fig. 8, they are the tilted angles -90° and $+90^\circ$. The output voltage on X and Y hotwires are recorded when the sensor is tilted around

the Y axis and the X axis, respectively. The output on the Z axis is recorded when the sensor is tilted around the X axis (see Fig. 6c).

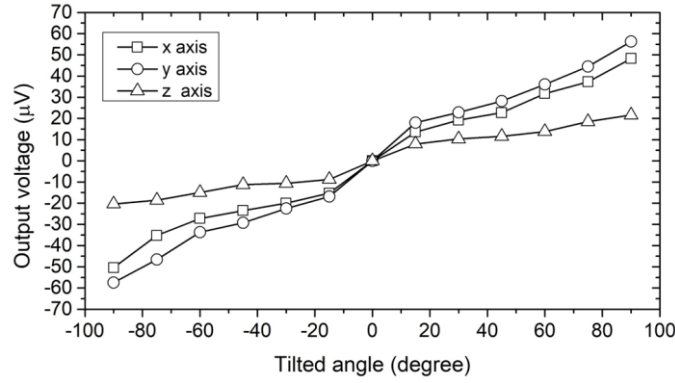


Figure 8. Output voltages on the X, Y, and Z hotwires while tilting around the X and Y axes.

The heater is heated with a constant current of 110 mA. The change in the heater resistance allows us to estimate the temperature of the heater by using the relation $\alpha\Delta T = \Delta R/R$, and its value is found to be approximately 70 °C. From Fig. 8, the sensitivities on the X axis and the Y axis are averaged as $V_{xx} = 0.62 \mu V/^\circ$ and $V_{yy} = 0.53 \mu V/^\circ$. The input of the Z hotwire while rotating around the X axis is $V_{zz} = 0.23 \mu V/^\circ$, which is of the same order as those of the X and Y axes. With the measured resistance at initial state of $R_x/R_z = 1.7$ (see part IV), the change in temperature in the hotwires X and Z is approximated as $\Delta T_x/\Delta T_z = (V_{xx}/V_{zz})/(R_x/R_z)$. For the result in Fig. 8, the temperature ΔT_x is 1.9 times higher than ΔT_z . This value relatively agrees with the simulation results presented in Figs. 2 and 3.

2. Effect of supply current on the heater

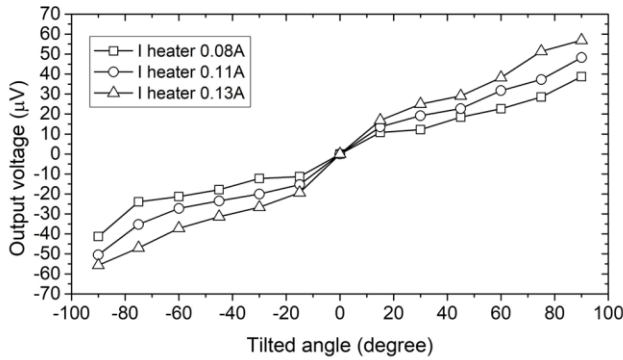


Figure 9. Effect of the heating current to the output voltage for the X axis sensing

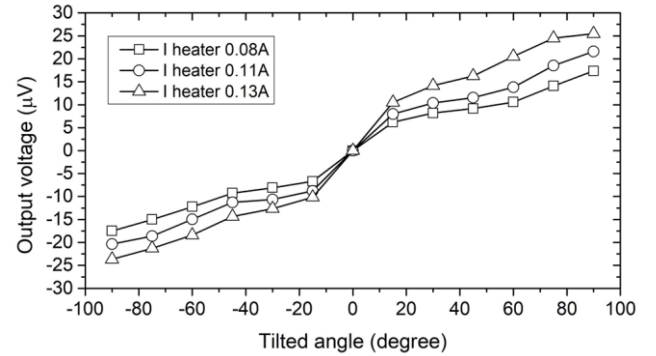


Figure 10. Effect of heating current to the output voltage for the Z axis sensing

The sensing ability of devices can be enhanced by increasing the temperature of the heater, since the temperature of the heater is directly related to how the medium can move inside the device [12,43]. A low temperature heater will significantly restrain the flow and degrade the sensor performance. The experiment was repeated in this study where the heater was subjected to three currents $I_h = 80$ mA, 110 mA, and 130 mA. The obtained results are shown in Figs. 9 and 10. It can be seen that when the current increases from 80 mA to 130 mA, the output increases by 127% of the magnitude for the X axis and by 146% for the Z axis. Therefore, the output voltages at the hotwires can be adjusted by the heater current, which can be used to accelerate the experiment.

3. Sensing linear acceleration

For the linear acceleration test, the output voltage is monitored while the sensor is placed at the edge of the turntable rotating at 135 rpm (centrifugal acceleration 0.89 g) and the heater is heated with a current $I_h = 110$ mA.

Figures 11 and 12 show the transient output voltage of the hotwires X_1 and X_2 when the acceleration is along the X and Z axes, respectively (see experimental setup in Fig. 6d). The changes between these two hotwires are almost similar in time, with a mismatch of only 210 ms at the left-peak slope. In Fig. 11, the two hotwires change their voltages opposite to each other, whereas in Fig. 12, their voltages change similarly, indicating that the heated air region changes the temperature of the X hotwire asymmetrically and symmetrically under the x and z applied accelerations, respectively.

The average noises are approximately 5 μV , significantly larger than the resolution of the 24-bit measuring device NI-9234 data acquisition. Therefore, the resolution of the sensor can be calculated as the signal-to-noise ratio, as shown in Figs. 11 and 12, and it is equivalent to 0.09g. The results also show very small drift evolution, nevertheless, the long-term drift evolution was not thoroughly tested for our device.

As the magnitudes of the voltages are almost the same in each case (Figs. 11 and 12), the effect of the Z acceleration can be cancelled out easily by means of a conventional electric circuit such as by forming half Wheatstone bridge by the pair of X hotwires. This kind of circuit is common in use in various sensing techniques, as reported in numerous literature [37],[39].

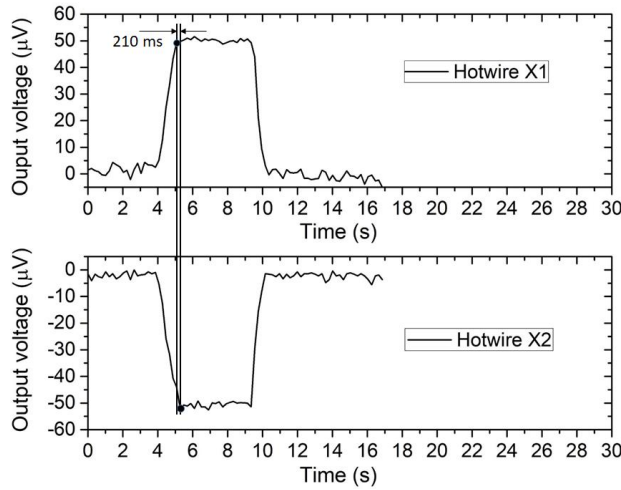


Figure 11. Transient response of the hotwires X with acceleration applied along the X axis.

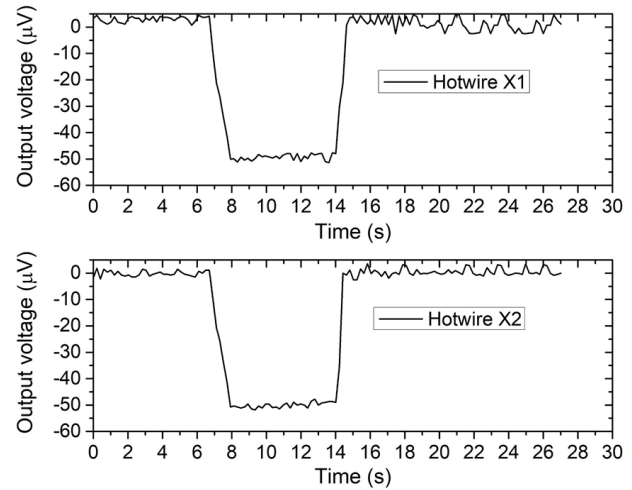


Figure 12. Transient response of the hotwires X with acceleration applied along the Z axis

Figure 13 shows the variation of the output voltage on the hotwires X with respect to the centrifugal acceleration applied to the X axis by the turntable (see Fig. 6d). The two X hotwires change their resistance opposingly when the scale factors of the hotwires X_1 and X_2 are $SF_{xx1} = -27.8 \mu\text{V/g}$ and $SF_{xx2} = +26.7 \mu\text{V/g}$, with the non-linearities (the ratio of output variation to maximum output full scale) of these output voltages being 2.7% and 2.2%, respectively.

The results depict that the output voltage changes linearly with the change of the rotation speed until the centrifugal acceleration reaches 21g. Meanwhile, the output voltage of the Z hotwire is significantly lower with the scale factor of $SF_{zx} = 2.2 \mu\text{V/g}$. These results indicate that the cross-sensitivity between the two axes is less than 8%, thereby closely matching with the simulation.

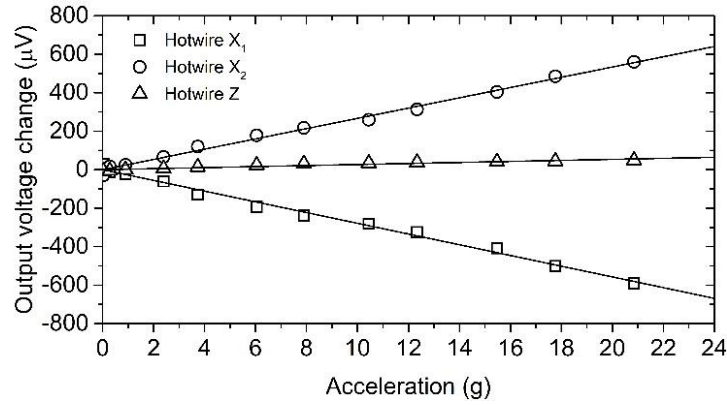


Figure 13. Output of the X axis and Z axis when the centrifugal acceleration is applied along the X axis by the turntable (rotating speed from 25 rpm to 700 rpm).

Similarly, Fig. 14 shows the output voltages of the hotwires in the X and Z axes while the centrifugal acceleration is applied to the Z axis (see the experimental setup in Fig. 6d). The two X hotwires are parallel with the plane of the turntable and should have similar response to the acceleration. This is confirmed by the data below where the two hotwires respond similarly. The scale factors of the X hotwire under Z acceleration are $SF_{xz1} = 37.7 \mu V/g$ and $SF_{xz2} = 37.5 \mu V/g$. If the X hotwires are conventionally connected by the half-bridge circuit, the total output of the X axis will be cancelled out (Fig. 14). In the meantime, the scale factor and the nonlinearity of Z hotwire under the Z acceleration are $SF_{zz} = 10.2 \mu V/g$ and 3.8%, respectively.

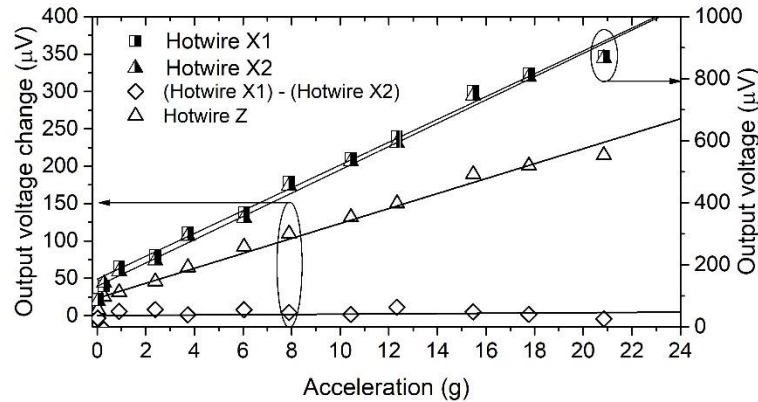


Figure 14. Output of the Z axis and the X axis when the centrifugal acceleration is applied along the Z axis by the turntable (rotating speed is from 25 rpm to 700 rpm and the current at the heater is $I_h = 110 \text{ mA}$)

Overall, the sensing performance of the present device is in the same order as the values in recent publications. In the simulation, the relative sensitivity of $\Delta T_z / \Delta T_x$ is in the same order with simulated result reported by other research group [58]. However, the sensing performance of the vertical acceleration of the presented device is less significantly affected by the horizontal acceleration. The performance of several published tri-axis convective accelerometers is summarized in Tab. 1. With these performing characteristic, the presented device and those sensors are in the same grade as classified in [59].

Table 1. Characteristics of some published tri-axis convective accelerometer

	X	Y	Z	V_{zx} (effect of a_x on the Z axis)
Bahari and Leung [36,37]	66 $\mu V/g$	64 $\mu V/g$	25 $\mu V/g$	84%
Rocha and Silva et al [38,39]	8.4 $\mu V/g$	7.9 $\mu V/g$	2.2 $\mu V/g$	Not reported
Maily and Nguyen et al [42,43]	7.2 mV/g	10 mV/g	0.4 mV/g	Not reported
This work	27.8 $\mu V/g$ (X)		10.2 $\mu V/g$	8%

It is worth noting that using the turntable to generate linear acceleration also induces Coriolis acceleration to the moving convective flow inside the device. The contribution of the Coriolis acceleration, however, is insignificant because the gravity driven flow has limited velocity in tiny confined space. The Coriolis acceleration is calculated as $2\vec{\omega} \times \vec{U}$ [60–64], where U is the velocity of flow inside the device and is estimated by simulation in order of millimeters per second (please refer to Fig. 2). The ratio of the centrifugal acceleration to the Coriolis acceleration, $\omega r_t/2U$, is therefore three orders of magnitude. Another concern in our experimental work is the output of tilting performance, which was not as linear as predicted by the simulation. The reasons are probably (i) the imperfection of the assembly process and (ii) the shape of the heater. While the circular-loop is ideal for the symmetry of device, it was not implemented for experimental measurement. We have confirmed by the simulation that the effect of the closed-loop heat source is more pronounced in the circular shape, however, the square shape heater in this work allows us to construct the sensor with cost-effective fabricating resource. These limitations can be improved by using micro fabrication process. As the sensor working principle relies on the heat transfer from the heater to the temperature sensing elements, optimizing the surrounding cavities and sensing element positions may further increase the sensitivity in all directions [45]. Finally, the sensor performance can be boosted by utilizing sensing element which has high resistance and temperature coefficient of resistance [14,17,60,61,65], or packing conditions such as pressure or high thermal conductivity gas [19,66–68].

VI. CONCLUSION

We reported a tri-axis convective accelerometer of millimeter-scale that utilizes a closed-loop heater to improve the sensing performance. The closed-loop heater concentrated the convectively heated air at the central part even though there was no heat source underneath, which helped to reduce the cross-effect of the horizontal acceleration to the vertical acceleration sensing. A numerical simulation was performed and the result was supported by the experimental work. The tilting test showed small cross-effect. The sensor was also tested by applying centrifugal acceleration and the linear relation between the output and the acceleration was achieved up to 20 g. The sensor was fabricated by additive manufacturing and the assembly process was simple, thus allowing quick and cost-effective prototyping to integrate this device into laboratory-scale projects. In addition, the device is made of laminated parts and can be potentially compatible with the conventional microfabrication process for significant reduction in the cost.

ACKNOWLEDGEMENT

This research is funded by the Vietnam National Foundation for Science and Technology Development (NAFOSTED) under grant number 107.01-2015.22

References

- [1] A. Albarbar, S.H. Teay, MEMS Accelerometers: Testing and Practical Approach for Smart Sensing and Machinery Diagnostics, in: Adv. Mechatronics MEMS Devices II. Microsystems Nanosyst., Springer, Cham, 2017: pp. 19–40. doi:10.1007/978-3-319-32180-6_2.
- [2] R. Dao, D.E. Morgan, H.H. Kries, David M. Bachelder, Ricardo Dao, Denny E. Morgan, Harold H. Kries, David M. Bachelder, Convective accelerometer and inclinometer, US5581034, 1996.
- [3] A.M. Leung, J. Jones, E. Czyzewska, J. Chen, B. Woods, Micromachined accelerometer based on convection heat transfer, in: Proc. MEMS 98. IEEE. Elev. Annu. Int. Work. Micro Electro Mech. Syst. An Investig. Micro Struct. Sensors, Actuators, Mach. Syst. (Cat. No.98CH36176), IEEE, 1998: pp. 627–630. doi:10.1109/MEMSYS.1998.659830.
- [4] S. Liu, R. Zhu, Micromachined Fluid Inertial Sensors, Sensors. 17 (2017) 367. doi:10.3390/s17020367.
- [5] V. Milanovic, E. Bowen, M.E. Zaghoul, N.H. Tea, J.S. Suehle, B. Payne, M. Gaitan, Micromachined convective accelerometers in standard integrated circuits technology, Appl. Phys. Lett. 76 (2000) 508. doi:10.1063/1.125803.
- [6] S. Billat, H. Glosch, M. Kunze, F. Hedrich, J. Frech, J. Auber, H. Sandmaier, W. Wimmer, W. Lang, Micromachined inclinometer with high sensitivity and very good stability, Sensors Actuators, A Phys. 97–98 (2002) 125–130. doi:10.1016/S0924-4247(01)00824-X.
- [7] F. Mailly, A. Martinez, A. Giani, F. Pascal-Delannoy, A. Boyer, Design of a micromachined thermal accelerometer: Thermal simulation and experimental results, Microelectronics J. 34 (2003) 275–280. doi:10.1016/S0026-2692(02)00194-5.
- [8] F. Mailly, A. Giani, A. Martinez, R. Bonnot, P. Temple-Boyer, A. Boyer, Micromachined thermal accelerometer, Sensors Actuators

- A Phys. 103 (2003) 359–363. doi:10.1016/S0924-4247(02)00428-4.
- [9] X.B. Luo, Z.X. Li, Z.Y. Guo, Y.J. Yang, Study on linearity of a micromachined convective accelerometer, *Microelectron. Eng.* 65 (2002) 87–101. doi:10.1016/S0167-9317(02)00731-1.
- [10] R. Zhu, H.G. Ding, Y. Su, Z.Y. Zhou, Micromachined gas inertial sensor based on convection heat transfer, *Sensors and Actuators a-Physical*. 130 (2006) 68–74. doi:10.1016/j.sna.2005.11.022.
- [11] D.S. Lee, Thermal accelerometer based predictive drop sensor, *Sensors Actuators, A Phys.* 135 (2007) 889–894. doi:10.1016/j.sna.2006.09.023.
- [12] V.T. Dau, D. Viet Dao, S. Sugiyama, A 2-DOF convective micro accelerometer with a low thermal stress sensing element, *Smart Mater. Struct.* 16 (2007) 2308–2314. doi:10.1088/0964-1726/16/6/034.
- [13] V.T. Dau, D.V. Dao, M. Hayashida, T.X. Dinh, S. Sugiyama, A Dual Axis Accelerometer Utilizing Low Doped Silicon Thermistor, *IEEE Trans. Sensors Micromachines*. 126 (2006) 190–194. doi:10.1541/ieejsmas.126.190.
- [14] V.T. Dau, D.V. Dao, T. Shiozawa, S. Sugiyama, Convective Gas Gyroscope Based on Thermo-Resistive Effect in Si P-N Junction, in: *TRANSDUCERS 2007 - 2007 Int. Solid-State Sensors, Actuators Microsystems Conf., IEEE, 2007*: pp. 2525–2528. doi:10.1109/SENSOR.2007.4300685.
- [15] V.T. Dau, T. Otake, T.X. Dinh, D.V. Dao, S. Sugiyama, A multi axis fluidic inertial sensor, in: *Proc. IEEE Sensors, IEEE, 2008*: pp. 666–669. doi:10.1109/ICSENS.2008.4716529.
- [16] V.T. Dau, T. Otake, T.X. Dinh, S. Sugiyama, Design and fabrication of convective inertial sensor consisting of 3DOF gyroscope and 2DOF accelerometer, in: *TRANSDUCERS 2009 - 2009 Int. Solid-State Sensors, Actuators Microsystems Conf., IEEE, 2009*: pp. 1170–1173. doi:10.1109/SENSOR.2009.5285911.
- [17] M. Han, J.-K. Kim, G.-M. Bae, Y. Bang, G.S. Lee, S.-W. Kang, D. Jung, Sensitivity improvement of a thermal convection-based tilt sensor using carbon nanotube, *Jpn. J. Appl. Phys.* 56 (2017) 06GF05. doi:10.7567/JJAP.56.06GF05.
- [18] M. Han, J.K. Kim, J.H. Park, W. Kim, S.W. Kang, S.H. Kong, D. Jung, Sensitivity and frequency-response improvement of a thermal convection-based accelerometer, *Sensors (Switzerland)*. 17 (2017). doi:10.3390/s17081765.
- [19] F. Mailly, A. Martinez, A. Giani, F. Pascal-Delannoy, A. Boyer, Effect of gas pressure on the sensitivity of a micromachined thermal accelerometer, *Sensors Actuators, A Phys.* 109 (2003) 88–94. doi:10.1016/j.sna.2003.09.025.
- [20] A. Garraud, P. Combette, J. Courteaud, A. Giani, Effect of the Detector Width and Gas Pressure on the Frequency Response of a Micromachined Thermal Accelerometer, *Micromachines*. 2 (2011) 167–178. doi:10.3390/mi2020167.
- [21] L. Lin, J. Jones, A liquid-filled buoyancy-driven convective micromachined accelerometer, *J. Microelectromechanical Syst.* 14 (2005) 1061–1069. doi:10.1109/JMEMS.2005.856651.
- [22] G. Kaltsas, D. Goustouridis, A.G. Nassiopoulou, A thermal convective accelerometer system based on a silicon sensor — Study and packaging, *Sensors And Actuators*. 132 (2006) 147–153. doi:10.1016/j.sna.2006.04.026.
- [23] X.B. Luo, Z.X. Li, Z.Y. Guo, Y.J. Yang, Thermal optimization on micromachined convective accelerometer, *Heat Mass Transf.* 38 (2002) 705–712. doi:10.1007/s002310100266.
- [24] K.-M. Liao, R. Chen, B.C.S. Chou, A novel thermal-bubble-based micromachined accelerometer, *Sensors Actuators A Phys.* 130–131 (2006) 282–289. doi:10.1016/j.sna.2006.02.049.
- [25] J. Bahari, J.D. Jones, A.M. Leung, Sensitivity improvement of micromachined convective accelerometers, *J. Microelectromechanical Syst.* 21 (2012) 646–655. doi:10.1109/JMEMS.2012.2189366.
- [26] O. Leman, F. Mailly, L. Latorre, P. Nouet, Noise analysis of a first-order thermal $\Sigma\Delta$ architecture for convective accelerometers, *Analog Integr. Circuits Signal Process.* 63 (2010) 415–423. doi:10.1007/s10470-009-9419-2.
- [27] A. Garraud, P. Loisel, A. Giani, P. Combette, A. Deblonde, Closed-loop micromachined accelerometer based on thermal convection, *Micro Nano Lett.* 7 (2012) 1092–1093. doi:10.1049/mnl.2012.0702.
- [28] J. Lin, C. Lin, C. Lin, A Novel Reliable and Low-Cost Wireless Thermal Convection-Type Angular Accelerometer Made Directly on a Flexible Substrate, *Sensors Mater.* 27 (2015) 743–754. doi:10.18494/SAM.2015.1111.
- [29] B. Mezghani, F. Tounsi, M. Masmoudi, Convection behavior analysis of CMOS MEMS thermal accelerometers using FEM and Hardee’s model, *Analog Integr. Circuits Signal Process.* 78 (2014) 301–311. doi:10.1007/s10470-013-0208-6.
- [30] B. Mezghani, F. Tounsi, M. Masmoudi, Development of an accurate heat conduction model for micromachined convective accelerometers, *Microsyst. Technol.* 21 (2015) 345–353. doi:10.1007/s00542-014-2079-x.
- [31] O. Leman, F. Mailly, L. Latorre, P. Nouet, HDL modeling of convective accelerometers for system design and optimization, *Sensors Actuators A Phys.* 142 (2008) 178–184. doi:10.1016/j.sna.2007.07.034.
- [32] A.A. Rekik, F. Azais, N. Dumas, F. Mailly, P. Nouet, A Behavioral Model of MEMS Convective Accelerometers for the Evaluation of Design and Calibration Strategies at System Level, *J. Electron. Test.* 27 (2011) 411–423. doi:10.1007/s10836-011-5207-x.
- [33] Memsic accelerometer, (n.d.). <http://www.memsic.com/accelerometers/> (accessed May 6, 2017).
- [34] A. Chaehoi, F. Mailly, L. Latorre, P. Nouet, Experimental and finite-element study of convective accelerometer on CMOS, *Sensors Actuators, A Phys.* 132 (2006) 78–84. doi:10.1016/j.sna.2006.04.057.
- [35] A.A. Rekik, F. Azais, F. Mailly, P. Nouet, Design-for-manufacturability of MEMS convective accelerometers through adaptive electrical calibration strategy, in: *2012 13th Lat. Am. Test Work., IEEE, 2012*: pp. 1–6. doi:10.1109/LATW.2012.6261237.
- [36] See-Ho Tsang, Abdul Haseeb Ma, K.S. Karim, A. Parameswaran, A.M. Leung, Monolithically fabricated polymers 3-axis thermal accelerometers designed for automated wirebond assembly, in: *2008 IEEE 21st Int. Conf. Micro Electro Mech. Syst., IEEE, 2008*: pp. 880–883. doi:10.1109/MEMSYS.2008.4443797.
- [37] J. Bahari, A.M. Leung, Micromachined three-axis thermal accelerometer with a single composite heater, *J. Micromechanics Microengineering*. 21 (2011) 75025. doi:10.1088/0960-1317/21/7/075025.

- [38] L.A. Rocha, C.S. Silva, M.F. Cerqueira, J.F. Ribeiro, L.M. Goncalves, A.J. Pontes, J.C. Viana, A microinjected 3-axis thermal accelerometer, *Procedia Eng.* 25 (2011) 607–610. doi:10.1016/j.proeng.2011.12.151.
- [39] C. Silva, J. Noh, H. Fonseca, A. Pontes, J. Gaspar, L.A. Rocha, Fabrication and characterization of polymeric three-axis thermal accelerometers, *J. Micromechanics Microengineering*. 25 (2015) 85005. doi:10.1088/0960-1317/25/8/085005.
- [40] L.A. Rocha, C.S. Silva, A.J. Pontes, J.C. Viana, Design of a 3-axis thermal accelerometer using an electro-thermo-fluidic model, in: 2012 13th Int. Therm. Mech. Multi-Physics Simul. Exp. Microelectron. Microsystems, IEEE, 2012: p. 1/4-4/4. doi:10.1109/ESimE.2012.6191775.
- [41] C.S. Silva, R.A. Dias, J.C. Viana, A.J. Pontes, L.A. Rocha, Static and dynamic modeling of a 3-axis thermal accelerometer, *Procedia Eng.* 47 (2012) 973–976. doi:10.1016/j.proeng.2012.09.309.
- [42] F. Mailly, H.B. Nguyen, L. Latorre, P. Nouet, CMOS implementation of a 3-axis thermal convective accelerometer, in: IEEE SENSORS 2014 Proc., IEEE, 2014: pp. 1471–1474. doi:10.1109/ICSENS.2014.6985292.
- [43] H.B. Nguyen, F. Mailly, L. Latorre, P. Nouet, A new monolithic 3-axis thermal convective accelerometer: principle, design, fabrication and characterization, *Microsyst. Technol.* (2014) 1–11. doi:10.1007/s00542-014-2254-0.
- [44] MXR9159, MEMSIC, (2007). http://www.memsic.com/userfiles/files/Datasheets/Accelerometer-Datasheets/MXR9150GM__Rev_D.pdf (accessed December 11, 2017).
- [45] Y. Hua, L. Jiang, Y. Cai, A. Leung, Y. Zhao, Single chip tri-axis accelerometer, US7424826, 2008.
- [46] Y. Ogami, T.X. Dinh, Convective Accelerometer (熱感知型加速度センサ), Japanese patent application JP 2013-96936A, 2013.
- [47] Y. Ogami, N. Murakita, K. Fukudome, Computational Experiments on the Step and Frequency Responses of a Three-Axis Thermal Accelerometer, *Sensors*. 17 (2017) 2618. doi:10.3390/s17112618.
- [48] M. Corcione, Effects of the thermal boundary conditions at the sidewalls upon natural convection in rectangular enclosures heated from below and cooled from above, *Int. J. Therm. Sci.* 42 (2003) 199–208. doi:10.1016/S1290-0729(02)00019-4.
- [49] A. Kondrashov, E. Burkova, Stationary convective regimes in a thin vertical layer under the local heating from below, *Int. J. Heat Mass Transf.* 118 (2018) 58–65. doi:10.1016/j.ijheatmasstransfer.2017.10.096.
- [50] A. Kondrashov, I. Sboev, P. Dunaev, Heater shape effects on thermal plume formation, *Int. J. Therm. Sci.* 122 (2017) 85–91. doi:10.1016/j.ijthermalsci.2017.08.012.
- [51] R.H. Hernández, Natural convection in thermal plumes emerging from a single heat source, *Int. J. Therm. Sci.* 98 (2015) 81–89. doi:10.1016/j.ijthermalsci.2015.06.010.
- [52] I.E. Sarris, I. Lekakis, N.S. Vlachos, Natural convection in rectangular tanks heated locally from below, *Int. J. Heat Mass Transf.* 47 (2004) 3549–3563. doi:10.1016/j.ijheatmasstransfer.2003.12.022.
- [53] A. Kondrashov, I. Sboev, K. Rybkin, Effect of boundary conditions on thermal plume growth, *Heat Mass Transf. Und Stoffuebertragung*. 52 (2016) 1359–1368. doi:10.1007/s00231-015-1660-x.
- [54] A. Kondrashov, I. Sboev, P. Dunaev, Evolution of convective plumes adjacent to localized heat sources of various shapes, *Int. J. Heat Mass Transf.* 103 (2016) 298–304. doi:10.1016/j.ijheatmasstransfer.2016.07.065.
- [55] D.X. Thien, O. Yoshifumi, Design and analysis of a triple-axis thermal accelerometer, in: 2013 Seventh Int. Conf. Sens. Technol., IEEE, 2013: pp. 295–300. doi:10.1109/ICSENS.2013.6727662.
- [56] S. SOMA, Study on the fire-tornado at the former site of the Hifukusho, *J. Geogr. (Chigaku Zasshi)*, Japanese. 84 (1975) 204–217. doi:10.5026/jgeography.84.4_204.
- [57] K. Kuwahara, Y. Oshima, Thermal Convection Caused by Ring-Type Heat Source, *J. Phys. Soc. Japan*. 51 (1982) 3711–3719. doi:10.1143/JPSJ.51.3711.
- [58] C.S. Silva, R.A. Dias, J.C. Viana, A.J. Pontes, L.A. Rocha, Static and dynamic modeling of a 3-axis thermal accelerometer, *Procedia Eng.* 47 (2012) 973–976. doi:10.1016/j.proeng.2012.09.309.
- [59] N. Yazdi, F. Ayazi, K. Najafi, Micromachined inertial sensors, *Proc. IEEE*. 86 (1998) 1640–1659. doi:10.1109/5.704269.
- [60] V.T. Dau, D.V. Dao, T. Shiozawa, H. Kumagai, S. Sugiyama, Development of a dual-axis thermal convective gas gyroscope, *J. Micromechanics Microengineering*. 16 (2006) 1301–1306. doi:10.1088/0960-1317/16/7/026.
- [61] V.T. Dau, D.V. Dao, T. Shiozawa, H. Kumagai, S. Sugiyama, A Single-Axis Thermal Convective Gas Gyroscope, *Sensors Mater.* 17 (2005) 453–463. <http://www.scopus.com/inward/record.url?eid=2-s2.0-3364552249&partnerID=MN8TOARS>.
- [62] V.T. Dau, T.X. Dinh, D.V. Dao, S. Sugiyama, Design and Simulation of a Novel 3-DOF MEMS Convective Gyroscope, *IEEJ Trans. Sensors Micromachines*. 128 (2008) 219–224. doi:10.1541/ieejsmas.128.219.
- [63] V.T. Dau, T.X. Dinh, C.D. Tran, P.N. Bui, D.D. Vien, H.T. Phan, Fluidic mechanism for dual-axis gyroscope, *Mech. Syst. Signal Process.* 108 (2018) 73–87. doi:10.1016/j.ymssp.2018.02.017.
- [64] P.T. Hoa, T.X. Dinh, V.T. Dau, Design Study of Multidirectional Jet Flow for a Triple-Axis Fluidic Gyroscope, *IEEE Sens. J.* 15 (2015) 4103–4113. doi:10.1109/JSEN.2015.2411631.
- [65] V.T. Dau, C.D. Tran, T.T. Bui, V.D.X. Nguyen, T.X. Dinh, Piezo-resistive and thermo-resistance effects of highly-aligned CNT based macrostructures, *RSC Adv.* 6 (2016) 106090–106095. doi:10.1039/C6RA22872K.
- [66] R. Mukherjee, P. Mandal, P.K. Guha, Sensitivity improvement of a dual axis thermal accelerometer with modified cavity structure, *Microsyst. Technol.* 23 (2017) 5357–5363. doi:10.1007/s00542-017-3338-4.
- [67] R. Mukherjee, J. Basu, P. Mandal, P.K. Guha, A review of micromachined thermal accelerometers, *J. Micromechanics Microengineering*. 27 (2017) 123002. doi:10.1088/1361-6439/aa964d.
- [68] P.F. Hodnett, Natural convection between horizontal heated concentric circular cylinders, *Zeitschrift Für Angew. Math. Und Phys.* ZAMP. 24 (1973) 507–516. doi:10.1007/BF01588154.